Dear Editors:

Thank you very much for your careful review and helpful comments for improving our manuscript acp-2019-758. We have accordingly made the careful revisions. Revised portions are highlighted in the revised manuscript. In the following we quoted each review question in the square brackets and added our response after each paragraph.

[1. Page 2. Line 21. change "observational" to "observed".]

Response 1: It has been changed.

[2. Page 2. Line 35-36. remove "that contributes...YRMB area"]

Response 2: It has been removed.

[3. Page 3. Line 43. remove "traffic".]

Response 3: It has been removed.

[4. Page 3. Line 60. "As of late"? do you understand what you mean]

Response 4: We have changed "As of late" to “Over recent years”.

[5. Page 4. Line 69. "The emissions factor includes ...". This statement is not correct. "chemical production and transformation" should not be counted in emissions.]

Response 5: We have corrected the sentence to “The emission factor includes emission source strength of air pollutants and the precursors” and moved the

"chemical transformation" into the following sentence.

[6. Page 6. Line 106. add "of" in-between "one which".]

Response 6: It has been corrected.

[7. Page 7. Line 139. change "coupled offline with" to "driven by"]

Response 7: It has been changed.

[8. Page 8. Line 161-162. It worths to give a bit more detail on the performance for different variables and sites for people who do not know much about the Taylor diagram.]

Response 8: Many thanks for the editor's careful review. The performance for different variables of air temperature, wind speed, relative humidity and air pressure at five sites over CEC was validated with standard deviation and the normalized root-mean-square error between simulations and observations in the Taylor diagram. Please the detail on the performance in the caption of Fig. 2.

[9. Page 9. Line 169-170. Please explain how you determine the residence time.]

Response 9: Many thanks for the editor's careful review. We have explained the residence time calculation as follows:

Stohl et al. (2005) mathematically derived the residence time for particles out of FLEXPART. Generally, in the backward trajectory of FLEXPART modeling, many particles are released at a receptor and transported backward in time. Then the residence time (not the lifetime) of all particles, normalized by the total number of released particles, is determined on a uniform grid.

References

Stohl, A., Forster, C., Frank, A., Seibert, P., and Wotawa, G.: Technical note: The Lagrangian particle dispersion model FLEXPART version 6.2, Atmospheric Chemistry & Physics, 5, 2461-2474, https://doi.org/10.5194/acp-5-2461-2005, 2015.

[10. Page 9. Line 172. add "as" after "considered"]

Response 10: It has been corrected.

[11. Page 9. Line 179. "h" to "hour"]

Response 11: It has been corrected.

[12. Page 9. Line 184-186. "The primary $PM_{2.5}$ emission data..." Does MEIC provide $PM_{2.5}$ emissions? or emissions for BC, SO_2,]

Response 12: Many thanks for the editor's careful review. MEIC provide 10 major atmospheric pollutants and greenhouse gases (included SO_2, NOx, CO, NMVOC, NH_3, CO_2, primary $PM_{2.5}$, primary PM_{10}, BC and OC), and it can be found in the MEIC website (http://www.meicmodel.org/about.html).

[13. Page 11. Line 214. remove "apparent"]

Response 13: It has been corrected.

[14. Page 12. Line 249. "precipitation could impact the emissions". How can precipitation impacts the emissions?]

Response 14: We have clarified with “precipitation could impact the emissions of fugitive dust” .

[15. Page 17. Line 350. change "exhibited" to "shown"]

Response 15: It has been corrected.

[16. Page 17. Figure 7a. Where do the PM2.5 concentrations (color contour in Figure 7a) come from?]

Response 16: The $PM_{2.5}$ concentrations were observed from the national air quality monitoring network operated by the Ministry of Ecology and Environment, China.

[17. Page 20. Line 412. move "in the YRMB area" to behind "the PM2.5 concentrations"]

Response 17: It has been corrected.

[18. Page 21. Line 425. Cite Gao et al. (2011) which had used the WRF-Chem to study the contributions of regional transport and other aerosol processes (emission, wet scavenging) to air pollution reduction in Beijing Olympic.

Gao, Y., X. Liu, C. Zhao, and M. Zhang (2011), Emission controls versus meteorological conditions in determining aerosol concentrations in Beijing during the 2008 Olympic Games, Atmospheric Chemistry and Physics, 11, 12437-12451.]

Response 18: Thanks for the article information. It has been cited.

Heavy air pollution with a unique "non-stagnant" atmospheric boundary layer in the Yangtze River Middle Basin aggravated by regional transport of $PM_{2.5}$ over China

Chao Yu[1,2], Tianliang Zhao[1, *], Yongqing Bai[3, *], Lei Zhang[1,4], Shaofei Kong[5], Xingna Yu[1], Jinhai He[1], Chunguang Cui[3], Jie Yang[1], Yinchang You[1], Guoxu Ma[1], Ming Wu[1], Jiacheng Chang[1]

1 Collaborative Innovation Center on Forecast and Evaluation of Meteorological Disasters, Key Laboratory for Aerosol-Cloud-Precipitation of China Meteorological Administration, PREMIC, Nanjing University of Information Science and Technology, Nanjing 210044, China

2 Southwest Electric Power Design Institute Co., Ltd of China Power Engineering Consulting Group, Chengdu, 610021, China

3 Institute of Heavy Rain, China Meteorological Administration, Wuhan, 430205, China

4 Chengdu Academy of Environmental Sciences, Chengdu, 610031, China

5 Department of Atmospheric Sciences, School of Environmental Studies, China University of Geosciences (Wuhan), 430074, Wuhan, China

* *Correspondence*: Tianliang Zhao (tlzhao@nuist.edu.cn); Yongqing Bai (2007byq@163.com)

Abstract: The regional transport of air pollutants, controlled by emission sources and meteorological factors, results in a complex source-receptor relationship of air pollution change. Wuhan, a metropolis in the Yangtze River Middle Basin (YRMB) of Central China, experienced

heavy air pollution characterized by hourly $PM_{2.5}$ concentrations reaching 471.1 μg m^{-3} in January 2016. To investigate the regional transport of $PM_{2.5}$ over central-eastern China (CEC) and the meteorological impact on wintertime air pollution in the YRMB area, ~~observational~~ observed meteorological and other relevant environmental data from January 2016 were analyzed. Our analysis presented noteworthy cases of heavy $PM_{2.5}$ pollution in the YRMB area with unique "non-stagnant" meteorological conditions of strong northerly winds, no temperature inversion, and additional unstable structures in the atmospheric boundary layer. This unique set of conditions differed from the stagnant meteorological conditions characterized by near-surface weak winds, air temperature inversion, and stable structure in the boundary layer that are typically observed in heavy air pollution over most regions in China. The regional transport of $PM_{2.5}$ over CEC aggravated $PM_{2.5}$ levels, thus creating heavy air pollution in the YRMB area. This demonstrates a source-receptor relationship between the originating air pollution regions in CEC and the receiving YRMB region. Furthermore, a backward trajectory simulation using a FLEXPART-WRF model to integrate the air pollutant emission inventory over China was used to explore the patterns of regional transport of $PM_{2.5}$ governed by the strong northerly winds in the cold air activity of the East Asian winter monsoon season ~~that contributes markedly to the heavy $PM_{2.5}$ pollution in the YRMB area~~. It was estimated that the regional transport of $PM_{2.5}$ from non-local air pollutant emissions contributes more than 65% of the $PM_{2.5}$ concentrations to the heavy air pollution in the YRMB region during the study period, revealing the importance of the regional transport of air pollutants over China as a causative factor of heavy air pollution over the YRMB area.

Key words: $PM_{2.5}$ pollution; Yangtze River Middle Basin; meteorological condition; regional transport; FLEXPART-WRF

1. Introduction

Haze pollution can result in serious environmental problems that adversely influence ~~traffic,~~ human health, climate change, and other significant aspects (An et al., 2019; Fuzzi et al., 2015; Nel, 2005). Based on observations in China, there is a well-established association between haze pollution and high concentrations of $PM_{2.5}$ (particulate matter with an aerodynamic diameter equal to or less than 2.5 μm). Air pollution levels are highly dependent on the emissions of air pollutants and changes in meteorology (An et al., 2019; Tie et al., 2017; Xu et al., 2016a; Xu et al., 2016b). The accumulation, maintenance, and dissipation of haze pollution events are generally determined by meteorological changes (Zhang et al., 2013; Zhang et al., 2015), among which boundary layer structures play the most important role (Zhao et al., 2013). Meteorological conditions of stagnation, characterized by near-surface low winds, high humidity, and stable boundary layers, could govern the periodic variations of haze pollution, which present as typical wintertime air pollution in China (Huang et al., 2018; Xu et al., 2016b; Zhang et al., 2013). Major anthropogenic pollutant sources exist over the vast flatland in central-eastern China (CEC), from the eastern edges of the Tibetan Plateau and the Loess Plateau to China's Pacific coast. In the CEC, four major regions of emission sources that exhibit haze pollution with excessive $PM_{2.5}$ concentrations and overall poor air quality are centered over the North China Plain (NCP), the Yangtze River Delta (YRD) in East China, the Pearl River Delta (PRD) in South China, and the Sichuan Basin (SCB) in Southwest China. Over recent years, ~~As of late, s~~Ssevere haze pollution events that have swept over much of CEC have been attributed to the regional transport of air pollutants (Cheng et al., 2008; Deng et al., 2011; Qiao et al., 2019; Tie et al., 2017; Wang et al., 2016; Zhang et al., 2012). The regional transport of air pollutants with a source-receptor relationship is an important

157 issue in our understanding of changes in air quality.

158 The source-receptor relationship of air pollution describes the impacts of emissions from
159 an upwind source region to pollutant concentrations or deposition at a downwind receptor area
160 (Seibert and Frank, 2004). The regional transport of source-receptor air pollutants is generally
161 complicated by two types of factors: emissions and meteorology (Voulgarakis et al., 2010; Zhao et
162 al., 2012). The emission factor includes emission source strength of air pollutants and the
163 precursors. Meanwhile, the meteorological factor determines the transport pathway from the
164 source to receptor regions, exchanges between the boundary layer and free troposphere, the
165 chemical transformation and the removal processes occurring over the source and receptor regions
166 as well as along the transport pathways. Driven by atmospheric circulations, the regional transport
167 of $PM_{2.5}$ from source regions can deteriorate air quality in the downwind receptor regions, leading
168 to the regional haze pollution observed in a large area over China (Chang et al., 2018; He et al.,
169 2017; Hu et al., 2018; Jiang et al., 2015; Wang et al., 2014).

170 The Yangtze River Middle Basin (YRMB) covers the lower subbasin of two provinces,
171 Hubei and Hunan, in Central China. It is geographically surrounded by four major haze pollution
172 regions, the NCP to the north, the YRD to the east, the PRD to the south, and the SCB to the west
173 (Fig. 1a). Due to the specialized location of the YRMB as a regional air pollutant transport hub
174 with subbasin topography (Fig. 1b), the regional transport of air pollutants driven by the cold air
175 flows of East Asian winter monsoon over CEC can create a special source-receptor relationship
176 between the source regions of haze pollution in upstream and the downwind YRMB region
177 (Zhong et al., 2019). However, there are unresolved questions regarding the meteorological

178 processes involved in the regional transport of air pollutants and the patterns of regional transport
179 over CEC that may contribute to the air pollution changes observed in the YRMB area.

180 Wuhan, a metropolis located in the YRMB, has confronted environmental problems
181 associated with urban air pollution, especially the heavy $PM_{2.5}$ pollution events that occur
182 frequently in the winter (Gong et al., 2015; Xu et al., 2017). Local emissions of air pollutants from
183 urban transportation, industrial exhaust, and bio-combustion play an important role in the YRMB
184 urban air pollution (Acciai et al., 2017; Zhang et al., 2015). Previous observational and modeling
185 studies on air pollution in this area have been conducted (Wu et al., 2018; Zheng et al., 2019).
186 However, the regional transport routes of $PM_{2.5}$ across CEC are governed by meteorological
187 drivers and their contribution to air pollution over the YRMB area are poorly understood,
188 especially in relation to heavy air pollution events. This study selected Wuhan as a representative
189 area within the YRMB for investigating the meteorological changes of air pollution events in
190 January 2016 and assessing the contribution of regional transport of $PM_{2.5}$ over CEC to heavy air
191 pollution in the YRMB area.

192 ## 2. Data and methods

193 ### 2.1 Data

194 Wuhan, the capital of the Hubei province, is located across the Yangtze River where its
195 surrounding water network attributes to its humid environment (Fig. 1b). In order to analyze the
196 air quality changes in Wuhan, hourly concentrations of air pollutants, including $PM_{2.5}$ in January
197 2016, were collected from the national air quality monitoring network operated by the Ministry of
198 Ecology and Environment (http://www.mee.gov.cn/), including ten observational sites in Wuhan,

199 nine of which were urban sites in residential and industrial zones and one of which was suburban
200 (Fig. S1). The air quality observation data are released by the Ministry of Ecology ~~and~~
201 ~~Environmental~~and Environmental Protection under quality control that is based on China's
202 national standard of air quality observation.

203 The meteorological data of surface observations and air sounding in Wuhan and other
204 observatories in CEC were obtained from the Meteorological Data Sharing Network of China
205 Meteorological Administration (http://data.cma.cn/). The data selected for this study included air
206 temperature, relative humidity, air pressure, and wind speed and wind direction. In order to
207 analyze the meteorological variations in the atmospheric boundary layer at the time of our study,
208 we used data with temporal resolutions of 3 h for surface observations, and 12 h for sounding
209 observations.

210 The surface $PM_{2.5}$ concentrations, averaged over the ten observational sites in Wuhan, were
211 used to characterize the variations of air pollution in January 2016 over this urban area.
212 Correlation coefficients were calculated between the 10-site averages and the observed
213 meteorological elements, including wind speed and air temperature, in Wuhan to explore the local
214 meteorological influences on the changes of ambient $PM_{2.5}$ concentrations.

215 The ERA-Interim reanalysis data from the European Centre for Medium-Range Weather
216 Forecasts (ECMWF) (https://www.ecmwf.int/en/forecasts/datasets/reanalysis-datasets/) were
217 applied to explore the cold air flows of East Asian winter monsoonal winds in January 2016 and
218 their anomalies during heavy $PM_{2.5}$ pollution over CEC.

2.2 FLEXPART-WRF modeling

2.2.1 Model description

The Flexible Particle dispersion (FLEXPART) model (Stohl et al., 2003; Stohl et al., 2005) is a Lagrange particle diffusion model developed by the Norwegian Institute for Air Research (NIAR). In this model, the trajectory of a large number of particles released from a source is simulated, considering the processes of tracer transport, turbulent diffusion, and wet and dry depositions in the atmosphere (Brioude et al., 2013). Applying a backward trajectory simulation can determine the distribution of potential source regions that may have an impact on a target point or receptor region (Chen et al., 2017a; Chen et al., 2017b; Seibert and Frank, 2004; Zhai et al., 2016).

Initially, the FLEXPART model could be driven by the global reanalysis meteorological data obtained from the ECMWF or the National Centers of Environmental Prediction (NCEP). However, since this study focuses on the fine and multiscale modeling of air pollutant sources and regional transport, the FLEXPART model was driven by~~coupled offline with~~ the Weather Research and Forecasting (WRF) model to effectively devise the combined model FLEXPART-WRF (Fast and Easter, 2006; Brioude et al., 2013), which has been widely used to investigate the potential sources of air pollutants regarding environmental change (An et al., 2014; De Foy et al., 2011; Sauvage et al., 2017; Stohl et al., 2003).

2.2.2 WRF modeling configuration and meteorological validation

In this study, the WRF model was configured with two nested domains, coarse and fine. The

coarse domain covered the entirety of Asia with a 30 × 30 km horizontal resolution, and the nested fine domain included most of China and its surrounding regions with a 10 × 10 km horizontal resolution (Fig. S2). The physical parameterizations used in WRF modeling were selected with the Morrison microphysics scheme (Morrison et al., 2009), the Rapid Radiative Transfer Model (RRTM) scheme for long and short wave radiation (Mlawer et al., 1997), the Yonsei University (YSU) boundary layer scheme (Hong et al., 2006), the Grell 3D cumulus parameterization, and the Noah land surface scheme (Grell et al., 2005). Using the reanalysis meteorological data in the horizontal resolutions of 1°×1° obtained from NCEP for initial and boundary meteorological conditions, the WRF simulation ran 12 h each time, where the first 6 h simulations constituted spin-up time.

The WRF-simulated meteorological fields, which included wind speed and direction, air temperature, relative humidity, and air pressure, were compared with observations at five typical sites (Wuhan, Changsha, Hefei, Zhengzhou, and Nanchang) over CEC (Fig. 2). The correlation coefficients were calculated and found to pass the significance level of 0.001, and the normalized standardized deviations were determined to be low (Taylor, 2001) (Fig. 2). Based on these results, it was evaluated that the WRF modeled meteorology was reasonably consistent with observations and could be used to drive the FLEXPART backward trajectory simulation.

2.3 Estimating contribution of regional transport of $PM_{2.5}$ to air pollution

In the FLEXPART-WRF model, the trajectory of particles released from a source is simulated. Using this Lagrangian method could result in a Jacobian matrix (footprint) with units of mass per volume per unit flux. Stohl et al (2005) mathematically derived the residence time for particles out

of FLEXPART. Generally, in the backward trajectory of FLEXPART modeling, many particles are released at a receptor and transported backward in time. Then the residence time (not the lifetime) of all particles, normalized by the total number of released particles, is determined on a uniform grid. Selecting Wuhan as the receptor in the YRMB, the residence time for a thickness of 100 m above the surface was calculated and considered as the ‘‘footprint’’ (in units of s). By multiplying the residence time with the air pollutant emission flux in the respective grid cell (in units of μg m^{-2} s^{-1}) calculated from the air pollutant emission inventory of 2016 for China (http://www.meicmodel.org/), the emission source contribution (in units of μg m^{-2}) from this grid cell to the receptor's air pollution change could be estimated (Stohl et al., 2003; Stohl et al., 2005; Ding et al., 2009).

In this study, the FLEXPART-WRF simulation was conducted for a ~~48 h~~48-hour backward trajectory with the release of 50,000 air particles in the first h from Wuhan (30.61°N, 114.42°E) for three heavy pollution events in January 2016. The results were output with the residence time of air particles in a horizontal resolution of 0.1° × 0.1°. The simulations of particle residence time over the 48 h backward trajectory pathways were multiplied with the regional primary $PM_{2.5}$ emission fluxes to quantify the contribution of regional transport of $PM_{2.5}$ to air quality change in the YRMB area while identifying patterns of regional transport of $PM_{2.5}$ over CEC. The primary $PM_{2.5}$ emission data from the Multi-resolution Emission Inventory for China (MEIC) (http://www.meicmodel.org/) in 2016 were selected for use as the regional $PM_{2.5}$ emission fluxes in this study.

Based on this backward trajectory simulation, the upstream sources of $PM_{2.5}$ emissions for heavy air pollution in Wuhan were identified. The contribution rates $\boldsymbol{rate_{i,j}}$ of regional transport of

$PM_{2.5}$ from the upstream sources to air pollution in the downstream receptor region of the YRMB were calculated by Eq. (1), and the total contribution ***R*** of regional transport from the non-local emission sources are estimated by Eq. (2) (Chen et al., 2017b; Ding et al., 2009).

$$rate_{i,j} = \frac{E_{i,j} \times r_{i,j}}{\sum_{1,1}^{N,S} E_{i,j} \times r_{i,j}} \qquad (1)$$

$$R = \sum_{(N_1,S_1)}^{(N_2,S_2)} rate_{i,j} \qquad (2)$$

where the subscripts ***i*** and **j** represent a grid location (***i, j***) over the 48 h backward trajectory from the first grid (***i***=1, ***j***=1) in Wuhan to the last grid (***i***=*N,* ***j***=*S*) over CEC; $\mathbf{r}_{i,j}$ represents the residence time of $PM_{2.5}$ particles simulated by FLEXPART-WRF; and $E_{i,j}$ represents the $PM_{2.5}$ emission flux over the grid. In Eq. (2), the first grid location (N_1, S_1) and the last grid location (N_2, S_2) over the non-local emission sources and the local area of Wuhan were determined, respectively, by the regional transport of $PM_{2.5}$ pathways and the YRMB area in Wuhan as simulated by the FLEXPART-WRF model.

3. Results and Discussion

3.1 Variations in local $PM_{2.5}$ concentrations and meteorology in January 2016

Based on the National Ambient Air Quality Standards of China released by the Ministry of Ecology and Environment in 2012 (http://www.mee.gov.cn/), light and heavy air pollution levels of $PM_{2.5}$ are categorized by the daily average $PM_{2.5}$ concentrations exceeding 75 and 150 μg m^{-3} in ambient air, respectively. The average monthly $PM_{2.5}$ concentration reached 105.8 μg m^{-3} in Wuhan, where the daily $PM_{2.5}$ concentrations exceeded 75 μg m^{-3} on 27 days during the entire month of January 2016 (Fig. 3a), indicating that this YRMB urban area was under significant

302 $PM_{2.5}$ pollution during this wintertime period. As shown in Figure 3a, a 21 day prolonged air
303 pollution event resulted from high levels of daily $PM_{2.5}$ concentrations (> 75 μg m^{-3}) from the 1st
304 to the 21st. During this period, three notably heavy air pollution events occurred on January 4th, the
305 10th to the 12th, and the 17th to the 18th with excessive daily $PM_{2.5}$ concentrations (>150 μg m^{-3}).
306 These three events are marked as P1, P2, and P3, respectively (Fig. 3b). Based on these
307 observations, we found the interesting phenomenon of an ~~apparent~~ approximately 7 day cycle of
308 heavy air pollution, reflecting an important modulation of meteorological oscillation in the East
309 Asian winter monsoonal winds affecting air pollution over the YRMB region (Xu et al., 2016a). A
310 period analysis on long-term observation data of air quality could provide further understanding
311 on air quality changes associated with meteorological drivers.

312 Figure 3b presents the hourly changes of $PM_{2.5}$ concentrations during the three heavy air
313 pollution events P1, P2, and P3. P1 began at 11:00 a.m. (local time is used for all events) and
314 ended at 11:00 p.m. the same day with an observed $PM_{2.5}$ concentration peak of 471.1 μg m^{-3}. P2
315 occurred from 10:00 p.m. on the 10th to 00:00 a.m. on the 12th. Over the 26 hour duration, it had
316 two peaks: 231.4 and 210.6 μg m^{-3}. P3 occurred between 7:00 p.m. on the 17th and 2:00 p.m. on
317 the 18th with an explosive growth rate of 42.9 μg m^{-3} h^{-1}. These events were characterized by short
318 durations of less than 26 h from rapid accumulation to fast dissipation.

319 The changes in $PM_{2.5}$ concentrations presented few differences between the suburban and
320 urban sites. Both had similar patterns and peaks of hourly changes during the heavy pollution
321 periods (Figs. S3, S4, and S5), demonstrating that regional heavy air pollution in a large area of
322 the YRMB region is, in part, due to regional transport over CEC. The only obvious differences in
323 air pollutant concentrations were measured during the clean air periods ($PM_{2.5}$ concentration < 75

μg m^{-3}) with the ~~relative~~relatively high and low concentrations of $PM_{2.5}$ at urban and suburban sites, respectively (Figs. S3, S4, and S5). This shows the important influence of high air pollutant emissions over urban areas on local air quality.

Using the environmental and meteorological data observed in Wuhan in January 2016, the effects of the meteorological conditions on $PM_{2.5}$ concentrations in the YRMB region were statistically analyzed in regard to hourly variations of surface $PM_{2.5}$ concentrations, near-surface wind speed (WS), wind direction (WD), surface air temperature (T) and pressure (P), and relative humidity (RH) (Fig. 4). Among the observed changes shown in Figure 4, the changes of $PM_{2.5}$ concentrations were found to have obviously positive correlations to T and RH, as well as a pronounced negative correlation to P and a weak positive correlation to WS (Table 1). There are several reasons for these results. Firstly, the lower WS could alter the concentrations of air pollutants with a weaker advection of cold air in conjunction with strong subsidence and stable atmospheric stratification, thus easily producing a stagnation area in the lower troposphere and resulting in regional pollutant accumulations for the development of haze events. Secondly, in the presence of high soil moisture, strong surface evaporation could increase the near-surface RH, which is conducive to the hygroscopic growth of participles for haze formation (Dawson et al., 2014; Xu et al., 2016a). Additionally, high air temperature and strong solar radiation could enhance chemical conversions for the formation of secondary aerosols in the atmosphere (He et al., 2012; Huang et al., 2014). Furthermore, precipitation could impact the emissions of fugitive dust and depositions of air pollutants (Dawson et al., 2007; Cheng et al., 2016). These observations could reflect the special influences of meteorological factors, such as winds, air temperature, humidity, and precipitation, on the physical and chemical processes in the ambient atmosphere that

affect air quality change in the YRMB region.

3.2 A unique meteorological condition of "non-stagnation" for heavy $PM_{2.5}$ pollution

3.2.1 Strong northerly winds

When we focused on the meteorological changes leading to high $PM_{2.5}$ levels exceeding 150 μg m^{-3} during the heavy air pollution events, it is noteworthy that all three episodes, P1, P2, and P3, were accompanied with strong WSs in the northerly direction, as well as evident turning points in prevailing conditions leading to falling T and increasing P (Fig. 4). The conditions observed during these episodes present the typical meteorological characteristics of cold air invasion with high air pressure over the East Asian monsoon region. The southward advance of a cold front could drive the regional transport of air pollutants over CEC (Kang et al., 2019). Climatologically, a strong northerly wind, low air temperature, and high air pressure are typical features of an incursion of cold air during the East Asian winter monsoon season that could disperse air pollutants, thus improving air quality in the NCP region (Miao et al., 2018; Xu et al., 2016b). This differs from the meteorological conditions of stagnation with weak winds observed for heavy air pollution events in the major air pollution regions of CEC (Ding et al., 2017;Huang et al., 2018), and the strong near-surface wind that anomalously accompanied the intensification of $PM_{2.5}$ during heavy air pollution periods over the study area (Fig. 4). This could imply that the regional air pollutant transport is worsening air quality over the YRMB, driven by the strong northerly winds during the East Asian winter monsoon season.

To further investigate the connection between meteorological elements in the near-surface

layer and changes in air quality affected by $PM_{2.5}$ concentrations in the YRMB region, we carried out a more detailed correlation analysis of $PM_{2.5}$ concentrations in Wuhan with WS and air temperature for three different levels of $PM_{2.5}$ concentrations: clean air environment ($PM_{2.5} < 75$ μg m^{-3}), light air pollution (75 μg $m^{-3} \leq PM_{2.5} < 150$ μg m^{-3}) and heavy air pollution ($PM_{2.5} \geq 150$ μg m^{-3}) periods (Table 2). The surface $PM_{2.5}$ concentrations were positively correlated with air temperature, and negatively correlated with wind speeds during the periods of clean air environment and light air pollution. It should be emphasized here that a significantly negative correlation (R = -0.19) of $PM_{2.5}$ concentrations to WS for the light air pollution period could indicate that weak winds are favorable for local $PM_{2.5}$ accumulation, reflecting an important effect of local air pollutant emissions on light air pollution periods over the YRMB area. In January 2016, the overall wind speed of Wuhan was weak with a monthly mean value of 2.0 m s^{-1}, which could help maintain the high $PM_{2.5}$ levels in the prolonged air pollution events experienced in the YRMB area. However, a significantly positive correlation (R = 0.41) existed between heavy air pollution levels of $PM_{2.5}$ concentrations ($PM_{2.5} > 150$ μg m^{-3}) and strong WSs during the heavy air pollution periods, which was inconsistent with the meteorological conditions of stagnation observed in the near-surface layer where weak winds were associated with heavy air pollution in East China (Cao et al., 2012; Deng et al., 2011). The meteorology and environment conditions in the YRMB region indicate the close association of heavy air pollution periods enhancing $PM_{2.5}$ concentrations with strong winds (Fig. 4, Table 2), therefore, reflecting a key role of regional transport of air pollutants in the development of the YRMB's heavy air pollution periods.

In order to clearly illustrate the impact of wind speed and direction on the $PM_{2.5}$ concentrations associated with the regional transport of upwind air pollutants, Figure 5 presents

389 the relation of hourly changes in surface $PM_{2.5}$ concentrations to WS and wind direction in Wuhan
390 during January 2016. As seen in Figure 5, strong northerly winds accompanied extremely high
391 $PM_{2.5}$ concentrations (> 150 μg m^{-3}) during the heavy air pollution periods, including a northeast
392 gale exceeding 5 m s^{-1} during the extreme heavy pollution periods with extremely high $PM_{2.5}$
393 concentrations (> 300 μg m^{-3}). These results reveal a unique meteorological condition of
394 "non-stagnation" with strong winds during events of heavy air pollution over the YRMB area.
395 Conversely, the observed $PM_{2.5}$ concentrations ranging between 75 and 150 μg m^{-3} for light air
396 pollution periods generally corresponded with low wind speeds (< 2 m s^{-1}) (Fig. 5). Therefore, it is
397 the meteorological condition of stagnation, characterized by weak winds, involved in the
398 accumulation of local air pollutants that is responsible for the light air pollution periods.
399 Meteorological impacts on air quality could include not only the stagnant condition of
400 meteorology with weak winds and stable boundary layer but also air temperature, humidity,
401 precipitation, and atmospheric radiation in close connection with atmospheric physical and
402 chemical processes. The meteorological drivers of air quality change are complicated by a series
403 of physical and chemical processes in the atmosphere, especially the formation of secondary air
404 pollutants with strong hygroscopic growth in the humid air environment overlying the dense water
405 network (Fig. 1b) in the YRMB region (Cheng et al., 2014; He et al., 2012; Huang et al., 2014).

406 ### 3.2.2 Unstable structures in the atmospheric boundary layer

407 The air sounding data observed in Wuhan were used to compare the structures of the
408 atmospheric boundary layer during the heavy air pollution and clean air periods. Figure 6 presents
409 the vertical profiles of air temperature, wind velocity, and potential temperature averaged for the
410 heavy $PM_{2.5}$ pollution and clean air periods in January 2016. It can be seen that the inversion layer

411 of air temperature did not exist during the heavy pollution periods, while a near-surface inversion
412 layer appeared at the height of about 200 m during the clean air periods (Fig. 6a). Compared to the
413 clean air period, the heavy air pollution events had stronger winds within the 1000 m layer but
414 weaker winds above the 1000 m layer (Fig. 6b), indicating that the regional transport of $PM_{2.5}$ was
415 mainly limited to the 1000 m layer, especially between 250 m and 800 m. These vertical structures
416 of horizontal wind could conduce to the downward mixing of the regionally transported air
417 pollutants and produce the near-surface accumulations of air pollutants over the YRMB area with
418 elevated ambient $PM_{2.5}$ concentrations, thus contributing to heavy air pollution.

419 To quantitatively characterize the stability of the atmospheric boundary layer, the vertical
420 profiles of potential air temperature (θ) were calculated with air temperature and pressure (Fig. 6c).
421 In this study, the vertical change rate of θ was used to quantify the static stability of the boundary
422 layer (Oke, 2002). A lower vertical change rate of θ generally indicates decreasing stability or
423 increasing instability of the boundary layer. The averaged static stability values of the near-surface
424 layer below a height of 200 m during the heavy pollution and clean air periods were
425 approximately 4.4 and 13.2 K km^{-1}, respectively (Table 3). This obvious decrease in stability of
426 the boundary layer from clean air to heavy pollution periods indicates an anomalous tendency of
427 the unstable boundary layer for the heavy pollution periods during January 2016 in the YRMB
428 area.

429 The meteorological conditions of stagnation characterized by weak wind, temperature
430 inversion, and a stable vertical structure of the atmospheric boundary layer are generally accepted
431 as the typical meteorological drivers for heavy air pollution (An et al., 2019; Ding et al., 2017).
432 Nevertheless, this study revealed a unique meteorological condition of “non-stagnation” in the

atmospheric boundary layer during heavy air pollution periods characterized by strong wind, lack of an inversion layer, and a more unstable structure of the atmospheric boundary layer. These "non-stagnant" meteorological conditions could be generally regarded as the typical pattern of atmospheric circulation that facilitates the regional transport of air pollutants from upstream sources to downwind receptor regions. The regional transport of $PM_{2.5}$ connected with the source-receptor relationship between the air pollution regions in CEC and the YRMB area was further investigated with the following observational and modeling analyses.

3.3 Regional transport of $PM_{2.5}$ in northerly winds observed over CEC

The monthly averages of $PM_{2.5}$ concentrations and the anomalies of wind speed averaged in three heavy air pollution periods relative to the monthly mean wind speed in January 2016 observed over CEC are ~~exhibited~~shown in Figure 7. Note that a large area of CEC experienced air pollution with high levels of $PM_{2.5}$ > 75 μg m^{-3} that were especially severe in the NCP region and the Fenhe-Weihe Plain in Central China (Fig. 7a). As seen in Figure 7, Wuhan (site 1 in Fig. 7a) and the surrounding YRMB region were situated in the downwind southern edge of the air pollution area blanketing CEC (Fig. 7a), where the northerly winds prevailed (Fig. 7b). Climatologically, CEC is a typical region of East Asian monsoons dominated with wintertime northerly winds (Ding, 1993). Note that the anomalously stronger northerly winds were observed over upstream CEC during the three periods of wintertime heavy $PM_{2.5}$ pollution (Fig. 7b). Driven by the stronger northerly winds, the regional transport of air pollutants from the source regions in windward CEC could largely contribute to heavy air pollution in the downwind receptor region of YRMB.

In order to explore the connection between the regional transport of $PM_{2.5}$ over CEC and the three events of heavy air pollution in the YRMB region, six observational sites were selected from the northwestern, northern, and northeastern directions over upstream CEC (Fig. 7a). These sites represent three different routes of the regional transport of $PM_{2.5}$ to Wuhan (site 1 in Fig. 7a) and are governed by the southward incursion of stronger northerly winds (Fig. 7b). Figure 8 presents the temporal changes of $PM_{2.5}$ concentration and wind speed along three typical routes of regional transport of $PM_{2.5}$ over CEC. The southeastward movement of heavy $PM_{2.5}$ pollution was driven by stronger northerly winds from Luoyang and Xinyang to Wuhan (sites 3, 2, and 1 in Fig. 7) and presented a northwestern route of regional transport of $PM_{2.5}$ for P1 (see upper panels of Fig. 8). The westward advance of $PM_{2.5}$ peaks was governed by the northeastern winds from Tongling and Hefei to Wuhan (sites 6, 5, and 1 in Fig. 7a). The regional transport of $PM_{2.5}$ across Eastern China to the YRMB in Central China exerted a significant impact on P2 (see middle panels of Fig. 8). A northern pathway of regional transport of $PM_{2.5}$ connected Zhengzhou and Xinyang to Wuhan (sites 4, 2, and 1 in Fig. 7a) during P3 with anomalously strong northerly winds (see Fig. 7b and lower panels of Fig. 8). Note, in Figure 8, that the heavy $PM_{2.5}$ pollution periods at the upstream sites of Hefei, Tongling, Luoyang, Xinyang, and Zhengzhou (sites 2-6 in Fig. 7a) were generally dispelled by strong northerly winds. At the same time, these winds could trigger the periods of heavy $PM_{2.5}$ pollution in the YRMB region (Wuhan, site 1 in Fig. 7a). Such inverse effects of strong winds on heavy air pollution in CEC and the YRMB region show the important role that regional transport of air pollutants can have in cleaning and worsening air pollution in the upstream CEC source regions and the downstream YRMB receptor region, respectively.

The regional transport over CEC that is associated with the source-receptor relationship

directing heavy $PM_{2.5}$ pollution to the YRMB region was revealed via observational analysis. The FLEXPART-WRF backward trajectory modeling was used to further identify the patterns of regional transport of $PM_{2.5}$ and estimate the resulting contribution to heavy air pollution in the YRMB region in the following section.

3.4 Contribution of regional transport of $PM_{2.5}$ to heavy pollution

In this study, for the receptor of Wuhan, the $PM_{2.5}$ contributions of regional transport over CEC to air pollution in the downwind receptor region could be approximately estimated. These estimations were based on the product of the residence time of air particles during regional transport as simulated by the FLEXPART-WRF model, and the $PM_{2.5}$ emission flux over the source grid in CEC determined by Eq. (1). The data yielded a so-called potential source contribution map, which is the geographical distribution of the regional transport contribution rates (%) of the emission source grid cell to $PM_{2.5}$ pollution at the receptor of Wuhan (Fig. 9).

The non-local emission sources that affected $PM_{2.5}$ concentrations during P1, P2, and P3 were quantified over CEC using the $PM_{2.5}$ contribution rates calculated with Eq. (1). Combining the distribution of high $PM_{2.5}$ contribution rates with the prevailing winds experienced during the three heavy $PM_{2.5}$ pollution periods, the major pathways of regional transport of $PM_{2.5}$ over CEC could be recognized (Fig. 9). During P1 in the YRMB region, the regional transport of air pollutants was centered along a northwestern route from the Fenhe-Weihe Plain in Central China, and a northeastern route from the YRD region in Eastern China (Fig. 9a). The YRD emission sources of air pollutants exerted a large impact on P2 through regional transport of $PM_{2.5}$ across Eastern China to the YRMB region along the north side of Yangtze River (Fig. 9b). Two major

497 regional transport pathways of $PM_{2.5}$ indicated by the spatial distribution of high contribution rates
498 of $PM_{2.5}$ from the NCP and YRD regions contributed to the elevated $PM_{2.5}$ concentrations during
499 P3 (Fig. 9c). Governed by the anomalous northerly winds in January 2016 (Fig. 7b), the regional
500 transport of $PM_{2.5}$ from the air pollutant emission source regions in CEC provided a significant
501 contribution to the wintertime heavy $PM_{2.5}$ pollution observed in the YRMB region (Figs. 7-9).
502 This was confirmed by the results of the FLEXPART-WRF backward trajectory simulation
503 utilized in this study.

504 The $PM_{2.5}$ contributions of regional transport over CEC to the $PM_{2.5}$ concentrations in the
505 YRMB area during P1, P2, and P3 ~~in the YRMB area~~ were estimated using Eq. (2) with the
506 resulting high contribution rates of 68.1%, 60.9%, and 65.3%, respectively (Table 4). The regional
507 transport of $PM_{2.5}$ from non-local air pollutant emissions could contribute more than 65% of the
508 $PM_{2.5}$ concentrations to the heavy air pollution in the YRMB region during the study period,
509 revealing a large contribution of regional transport of $PM_{2.5}$ over CEC to the enhancement of
510 $PM_{2.5}$ levels in the YRMB area for the wintertime heavy air pollution.

511 Note that the potential source contribution is estimated based on transport alone, ignoring
512 chemical and removal processes. We understand that these processes, including complex
513 deposition, and chemical conversion for the formation of secondary particles, were not introduced
514 in the FLEXPART-WRF simulation, which could represent the basic features of contribution and
515 patterns of regional $PM_{2.5}$ transport over CEC when limited to the primary $PM_{2.5}$ particles
516 highlighted in this study.

517 Normally researchers rely on 3-D numerical models with process analysis capability, such

as integrated process rates (IPRs), in order to quantify the contributions of regional transport to the occurrence of air pollution episodes (Gao et al., 2011; Hu et al., 2018; Jiang et al., 2015). In this study, simulations with a Lagrange particle dispersion FLEXPART-WRF model were utilized to calculate the percentage contribution of regional transport while identifying the transport pathway. The major uncertainty of this method for such calculations, as compared to other methods such as IPRs, is that the physical and chemical processes, including chemical conversion for the formation of secondary particles, were not introduced in the FLEXPART-WRF simulation. Considering that there is less precipitation in the winter monsoon season over CEC, this methodology has proven its robustness to quantify the regional transport contribution within the uncertainty range by relying on a portion of secondary organic and inorganic aerosols that resulted from the complex physical and chemical processes in the atmosphere.

4. Conclusions

This study investigated the ambient $PM_{2.5}$ variations over Wuhan, a typical YRMB area in Central China in January 2016, by analyzing the observational data of the environment and meteorology. In addition to this, we did a FLEXPART-WRF simulation to explore the meteorological processes involved in the regional transport of air pollutants, the regional transport patterns of $PM_{2.5}$, and how it contributes to heavy air pollution in the YRMB region. Focusing our study on three heavy $PM_{2.5}$ pollution periods we found a unique “non-stagnant” atmospheric boundary layer for wintertime heavy air pollution that was aggravated by the regional transport of $PM_{2.5}$ over CEC. This boundary layer was characterized by strong winds, no inversion layer, and a more unstable structure. These non-stagnant conditions during heavy air pollution periods with high $PM_{2.5}$ concentrations facilitate our understanding of the air pollutant source-receptor

relationship of regional transport in air quality change. Our study is of great interest to the air quality community given the unique features of the air pollution meteorology, which are very different from "stagnant" meteorological conditions presented in textbooks.

Although emissions and local accumulation of air pollutants can lead to the formation of light air pollution, in regard to $PM_{2.5}$ over the YRMB region, the regional transport of $PM_{2.5}$ from upstream source regions of air pollutant emissions in CEC contributed significantly (more than 65%) to the excessive $PM_{2.5}$ concentrations during wintertime heavy air pollution in the downwind YRMB region in January 2016, as governed by the strong northerly winds in the East Asian winter monsoon season over CEC.

Based on the variations of air quality and meteorology in a typical urban YRMB region, this study revealed a unique "non-stagnant" meteorological condition for heavy air pollution with a strong contribution of regional transport of $PM_{2.5}$ over China. These conditions and contributions can be investigated further with climate analyses of long-term observations and more comprehensive modeling of air quality and meteorology.

Data availability: The data used in this paper can be provided by Chao Yu (ychao012@foxmail.com) upon request.

Supplement: The supplement related to this article is available online at: https://doi.org/

Author contributions: CY, TZ, and YB conducted the study design. XY, LZ, and SK provided the observational data. LZ assisted with data processing. CY wrote the manuscript with the help of TZ and XY. YB, SK, JH, CC, JY, YY, GM, MW, and JC were involved in the scientific interpretation and discussion. All authors provided commentary on the paper.

Competing interests: The authors declare that they have no conflicts of interest.

Acknowledgement: This study was jointly funded by the National Natural Science Foundation of China (41830965; 91744209), the National Key R & D Program Pilot Projects of China (2016YFC0203304), and the Postgraduate Research & Practice Innovation Program of Jiangsu Province (KYCX18_1027).

References

Acciai, C., Zhang, Z., Wang, F., Zhong, Z., and Lonati, G.: Characteristics and source Analysis of trace Elements in $PM_{2.5}$ in the Urban Atmosphere of Wuhan in Spring, Aerosol and Air Quality Research, 17, 2224-2234, https://doi.org/10.4209/aaqr.2017.06.0207, 2017.

An, X., Yao, B., Li, Y., Li, N., and Zhou, L.: Tracking source area of Shangdianzi station using Lagrangian particle dispersion model of FLEXPART, Meteorological Applications, 21, 466-473, https://doi.org/10.1002/met.1358, 2014.

An, Z., Huang, R. J., Zhang, R., Tie, X., Li, G., Cao, J., Zhou, W., Shi, Z., Han, Y., Gu, Z., and Ji, Y.: Severe haze in northern China: A synergy of anthropogenic emissions and atmospheric processes, Proceedings of the National Academy of Sciences, 116, 8657-8666, https://doi.org/10.1073/pnas.1900125116, 2019.

581 Brioude, J., Arnold, D., Stohl, A., Cassiani, M., Morton, D., Seibert, P., Angevine, W., Evan, S.,
582 Dingwell, A., Fast, J. D., Easter, R. C., Pisso, I., Burkhart, J., and Wotawa, G.: The Lagrangian
583 particle dispersion model FLEXPART-WRF version 3.1, Geoscientific Model Development, 6,
584 1889-1904, https://doi.org/10.5194/gmd-6-1889-2013, 2013.
585 Cao, J.-j., Wang, Q.-y., Chow, J. C., Watson, J. G., Tie, X.-x., Shen, Z.-x., Wang, P., and An, Z.-s.:
586 Impacts of aerosol compositions on visibility impairment in Xi'an, China, Atmospheric
587 Environment, 59, 559-566, https://doi.org/10.1016/j.atmosenv.2012.05.036, 2012.
588 Chang, X., Wang, S., Zhao, B., Cai, S., and Hao, J.: Assessment of inter-city transport of
589 particulate matter in the Beijing-Tianjin-Hebei region, Atmospheric Chemistry and Physics, 18,
590 4843-4858, https://doi.org/10.5194/acp-18-4843-2018, 2018.
591 Chen, B., Xu, X.-D., and Zhao, T.: Quantifying oceanic moisture exports to mainland China in
592 association with summer precipitation, Climate Dynamics, 51, 4271-4286,
593 https://doi.org/10.1007/s00382-017-3925-1, 2017a.
594 Chen, S., Zhou, G., and Zhu, B.: A method for fast quantification of air pollutant sources (in
595 Chinese), Acta Scientiae Circumstantiae, 37, 2474-2481,
596 https://doi.org/10.13671/j.hjkxxb.2017.0045, 2017b.
597 Cheng, H., Gong, W., Wang, Z., Zhang, F., Wang, X., Lv, X., Liu, J., Fu, X., and Zhang, G.: Ionic
598 composition of submicron particles ($PM_{1.0}$) during the long-lasting haze period in January 2013 in
599 Wuhan, central China, Journal of Environmental Sciences, 26, 810-817,
600 https://doi.org/10.1016/s1001-0742(13)60503-3, 2014.
601 Cheng, X., Zhao, T., Gong, S., Xu, X., Han, Y., Yin, Y., Tang, L., He, H., and He, J.: Implications
602 of East Asian summer and winter monsoons for interannual aerosol variations over central-eastern

China, Atmospheric Environment, 129, 218-228, https://doi.org/10.1016/j.atmosenv.2016.01.037, 2016.

Cheng, Y. F., Wiedensohler, A., Eichler, H., Heintzenberg, J., Tesche, M., Ansmann, A., Wendisch, M., Su, H., Althausen, D., and Herrmann, H.: Relative humidity dependence of aerosol optical properties and direct radiative forcing in the surface boundary layer at Xinken in Pearl River Delta of China: An observation based numerical study, Atmospheric Environment, 42, 6373-6397, https://doi.org/10.1016/j.atmosenv.2008.04.009, 2008.

Dawson, J., Adams, P., and Pandis, S.: Sensitivity of $PM_{2.5}$ to climate in the Eastern US: a modeling case study, Atmospheric chemistry and physics, 7, 4295-4309, https://doi.org/10.5194/acp-7-4295-2007, 2007.

Dawson, J. P., Bloomer, B. J., Winner, D. A., and Weaver, C. P.: Understanding the Meteorological Drivers of U.S. Particulate Matter Concentrations in a Changing Climate, Bulletin of the American Meteorological Society, 95, 521-532, https://doi.org/10.1175/bams-d-12-00181.1, 2014.

De Foy, B., Burton, S. P., Ferrare, R. A., Hostetler, C. A., Hair, J. W., Wiedinmyer, C., and Molina, L. T.: Aerosol plume transport and transformation in high spectral resolution lidar measurements and WRF-Flexpart simulations during the MILAGRO Field Campaign, Atmospheric Chemistry and Physics, 11, 3543-3563, https://doi.org/10.5194/acp-11-3543-2011, 2011.

Deng, J., Wang, T., Jiang, Z., Xie, M., Zhang, R., Huang, X., and Zhu, J.: Characterization of visibility and its affecting factors over Nanjing, China, Atmospheric Research, 101, 681-691, https://doi.org/10.1016/j.atmosres.2011.04.016, 2011.

Ding, A., Wang, T., Xue, L., Gao, J., Stohl, A., Lei, H., Jin, D., Ren, Y., Wang, X., and Wei, X.: Transport of north China air pollution by midlatitude cyclones: Case study of aircraft

625 measurements in summer 2007, Journal of Geophysical Research: Atmospheres, 114,
626 https://doi.org/doi:10.1029/2008JD011023, 2009.
627 Ding, Y.: Monsoons over china, Springer Science & Business Media, 1993.
628 Ding, Y., Wu, P., Liu, Y., and Song, Y.: Environmental and Dynamic Conditions for the
629 Occurrence of Persistent Haze Events in North China, Engineering, 3, 266-271,
630 https://doi.org/10.1016/j.eng.2017.01.009, 2017.
631 Fast, J. D., and Easter, R. C.: A Lagrangian particle dispersion model compatible with WRF, 7th
632 WRF Users Workshop, NCAR, 2006, 19-22.
633 Fuzzi, S., Baltensperger, U., Carslaw, K., Decesari, S., Denier van der Gon, H., Facchini, M. C.,
634 Fowler, D., Koren, I., Langford, B., Lohmann, U., Nemitz, E., Pandis, S., Riipinen, I., Rudich, Y.,
635 Schaap, M., Slowik, J. G., Spracklen, D. V., Vignati, E., Wild, M., Williams, M., and Gilardoni, S.:
636 Particulate matter, air quality and climate: lessons learned and future needs, Atmospheric
637 Chemistry and Physics, 15, 8217-8299, https://doi.org/10.5194/acp-15-8217-2015, 2015.
638 Gao, Y., X. Liu, C. Zhao, and M. Zhang.: Emission controls versus meteorological conditions in
639 determining aerosol concentrations in Beijing during the 2008 Olympic Games, Atmospheric
640 Chemistry and Physics, 11, 12437-12451, https://doi.org/10.5194/acp-11-12437-2011, 2011.
641 Gong, W., Zhang, T., Zhu, Z., Ma, Y., Ma, X., and Wang, W.: Characteristics of $PM_{1.0}$, $PM_{2.5}$, and
642 PM_{10}, and Their Relation to Black Carbon in Wuhan, Central China, Atmosphere, 6, 1377-1387,
643 https://doi.org/10.3390/atmos6091377, 2015.
644 Grell, G. A., Peckham, S. E., Schmitz, R., McKeen, S. A., Frost, G., Skamarock, W. C., and Eder,
645 B.: Fully coupled "online" chemistry within the WRF model, Atmospheric Environment, 39,
646 6957-6975, https://doi.org/10.1016/j.atmosenv.2005.04.027, 2005.

He, J., Mao, H., Gong, S., Yu, Y., Wu, L., Liu, H., Chen, Y., Jing, B., Ren, P., and Zou, C.: Investigation of Particulate Matter Regional Transport in Beijing Based on Numerical Simulation, Aerosol and Air Quality Research, 17, 1181-1189, https://doi.org/10.4209/aaqr.2016.03.0110, 2017.

He, K., Zhao, Q., Ma, Y., Duan, F., Yang, F., Shi, Z., and Chen, G.: Spatial and seasonal variability of $PM_{2.5}$ acidity at two Chinese megacities: insights into the formation of secondary inorganic aerosols, Atmospheric Chemistry and Physics, 12, 1377-1395, https://doi.org/10.5194/acp-12-1377-2012, 2012.

Hong, S.-Y., Noh, Y., and Dudhia, J.: A new vertical diffusion package with an explicit treatment of entrainment processes, Monthly weather review, 134, 2318-2341, https://doi.org/10.1175/MWR3199.1,2006, 2006.

Hu, J., Li, Y., Zhao, T., Liu, J., Hu, X.-M., Liu, D., Jiang, Y., Xu, J., and Chang, L.: An important mechanism of regional O_3 transport for summer smog over the Yangtze River Delta in eastern China, Atmospheric Chemistry and Physics, 18, 16239-16251, https://doi.org/10.5194/acp-18-16239-2018, 2018.

Huang, Q., Cai, X., Wang, J., Song, Y., and Zhu, T.: Climatological study of the Boundary-layer air Stagnation Index for China and its relationship with air pollution, Atmospheric Chemistry and Physics, 18, 7573-7593, https://doi.org/10.5194/acp-18-7573-2018, 2018.

Huang, R. J., Zhang, Y., Bozzetti, C., Ho, K. F., Cao, J. J., Han, Y., Daellenbach, K. R., Slowik, J. G., Platt, S. M., Canonaco, F., Zotter, P., Wolf, R., Pieber, S. M., Bruns, E. A., Crippa, M., Ciarelli, G., Piazzalunga, A., Schwikowski, M., Abbaszade, G., Schnelle-Kreis, J., Zimmermann, R., An, Z., Szidat, S., Baltensperger, U., El Haddad, I., and Prevot, A. S.: High secondary aerosol contribution

669 to particulate pollution during haze events in China, Nature, 514, 218-222,
670 https://doi.org/10.1038/nature13774, 2014.
671 Jiang, C., Wang, H., Zhao, T., Li, T., and Che, H.: Modeling study of $PM_{2.5}$ pollutant transport
672 across cities in China's Jing-Jin-Ji region during a severe haze episode in December 2013,
673 Atmospheric Chemistry and Physics, 15, 5803-5814, https://doi.org/10.5194/acp-15-5803-2015,
674 2015.
675 Kang, H., Zhu, B., Gao, J., He, Y., Wang, H., Su, J., Pan, C., Zhu, T., and Yu, B.: Potential impacts
676 of cold frontal passage on air quality over the Yangtze River Delta, China, Atmospheric Chemistry
677 and Physics, 19, 3673-3685, https://doi.org/10.5194/acp-19-3673-2019, 2019.
678 Miao, Y., Guo, J., Liu, S., Zhao, C., Li, X., Zhang, G., Wei, W., and Ma, Y.: Impacts of synoptic
679 condition and planetary boundary layer structure on the trans-boundary aerosol transport from
680 Beijing-Tianjin-Hebei region to northeast China, Atmospheric Environment, 181, 1-11,
681 https://doi.org/10.1016/j.atmosenv.2018.03.005, 2018.
682 Mlawer, E. J., Taubman, S. J., Brown, P. D., Iacono, M. J., and Clough, S. A.: Radiative transfer
683 for inhomogeneous atmospheres: RRTM, a validated correlated-k model for the longwave, Journal
684 of Geophysical Research: Atmospheres, 102, 16663-16682, https://doi.org/10.1029/97jd00237,
685 1997.
686 Morrison, H., Thompson, G., and Tatarskii, V.: Impact of Cloud Microphysics on the Development
687 of Trailing Stratiform Precipitation in a Simulated Squall Line: Comparison of One- and
688 Two-Moment Schemes, Monthly Weather Review, 137, 991-1007,
689 https://doi.org/10.1175/2008mwr2556.1, 2009.
690 Nel, A.: Air pollution-related illness: effects of particles, Science, 308, 804-806,

https://doi.org/10.1126/science.1108752, 2005.

Oke, T. R.: Boundary layer climates, Routledge, 2002.

Qiao, X., Guo, H., Tang, Y., Wang, P., Deng, W., Zhao, X., Hu, J., Ying, Q., and Zhang, H.: Local and regional contributions to fine particulate matter in the 18 cities of Sichuan Basin, southwestern China, Atmospheric Chemistry and Physics, 19, 5791-5803, https://doi.org/10.5194/acp-19-5791-2019, 2019.

Sauvage, B., Fontaine, A., Eckhardt, S., Auby, A., Boulanger, D., Petetin, H., Paugam, R., Athier, G., Cousin, J.-M., Darras, S., Nédélec, P., Stohl, A., Turquety, S., Cammas, J.-P., and Thouret, V.: Source attribution using FLEXPART and carbon monoxide emission inventories: SOFT-IO version 1.0, Atmospheric Chemistry and Physics, 17, 15271-15292, https://doi.org/10.5194/acp-17-15271-2017, 2017.

Seibert, P., and Frank, A.: Source-receptor matrix calculation with a Lagrangian particle dispersion model in backward mode, Atmospheric Chemistry and Physics, 4, 51-63, https://doi.org/10.5194/acp-4-51-2004, 2004.

Stohl, A., Forster, C., Eckhardt, S., Spichtinger, N., Huntrieser, H., Heland, J., Schlager, H., Wilhelm, S., Arnold, F., and Cooper, O.: A backward modeling study of intercontinental pollution transport using aircraft measurements, Journal of Geophysical Research: Atmospheres, 108, https://doi.org/10.1029/2002jd002862, 2003.

Stohl, A., Forster, C., Frank, A., Seibert, P., and Wotawa, G.: Technical note: The Lagrangian particle dispersion model FLEXPART version 6.2, Atmospheric Chemistry & Physics, 5, 2461-2474, https://doi.org/10.5194/acp-5-2461-2005, 2005.

Taylor, K. E.: Summarizing multiple aspects of model performance in a single diagram, Journal of

713 Geophysical Research: Atmospheres, 106, 7183-7192, https://doi.org/10.1029/2000jd900719,
714 2001.
715 Tie, X., Huang, R. J., Cao, J., Zhang, Q., Cheng, Y., Su, H., Chang, D., Poschl, U., Hoffmann, T.,
716 Dusek, U., Li, G., Worsnop, D. R., and O'Dowd, C. D.: Severe Pollution in China Amplified by
717 Atmospheric Moisture, Science Report, 7, 15760, https://doi.org/10.1038/s41598-017-15909-1,
718 2017.
719 Voulgarakis, A., Savage, N., Wild, O., Braesicke, P., Young, P., Carver, G., and Pyle, J.:
720 Interannual variability of tropospheric composition: the influence of changes in emissions,
721 meteorology and clouds, Atmospheric Chemistry and Physics, 10, 2491-2506,
722 https://doi.org/10.5194/acp-10-2491-2010, 2010.
723 Wang, H. L., Qiao, L. P., Lou, S. R., Zhou, M., Ding, A. J., Huang, H. Y., Chen, J. M., Wang, Q.,
724 Tao, S. K., Chen, C. H., Li, L., and Huang, C.: Chemical composition of $PM_{2.5}$ and meteorological
725 impact among three years in urban Shanghai, China, Journal of Cleaner Production, 112,
726 1302-1311, https://doi.org/10.1016/j.jclepro.2015.04.099, 2016.
727 Wang, S. X., Zhao, B., Cai, S. Y., Klimont, Z., Nielsen, C. P., Morikawa, T., Woo, J. H., Kim, Y.,
728 Fu, X., Xu, J. Y., Hao, J. M., and He, K. B.: Emission trends and mitigation options for air
729 pollutants in East Asia, Atmospheric Chemistry and Physics, 14, 6571-6603,
730 https://doi.org/10.5194/acp-14-6571-2014, 2014.
731 Wu, J., Kong, S., Wu, F., Cheng, Y., Zheng, S., Yan, Q., Zheng, H., Yang, G., Zheng, M., Liu, D.,
732 Zhao, D., and Qi, S.: Estimating the open biomass burning emissions in central and eastern China
733 from 2003 to 2015 based on satellite observation, Atmospheric Chemistry and Physics, 18,
734 11623-11646, https://doi.org/10.5194/acp-18-11623-2018, 2018.

735 Xu, G., Jiao, L., Zhang, B., Zhao, S., Yuan, M., Gu, Y., Liu, J., and Tang, X.: Spatial and Temporal
736 Variability of the $PM_{2.5}/PM_{10}$ Ratio in Wuhan, Central China, Aerosol and Air Quality Research,
737 17, 741-751, https://doi.org/10.4209/aaqr.2016.09.0406, 2017.
738 Xu, J., Chang, L., Qu, Y., Yan, F., Wang, F., and Fu, Q.: The meteorological modulation on $PM_{2.5}$
739 interannual oscillation during 2013 to 2015 in Shanghai, China, Science of the Total Environment,
740 572, 1138-1149, https://doi.org/10.1016/j.scitotenv.2016.08.024, 2016a.
741 Xu, X., Zhao, T., Liu, F., Gong, S. L., Kristovich, D., Lu, C., Guo, Y., Cheng, X., Wang, Y., and
742 Ding, G.: Climate modulation of the Tibetan Plateau on haze in China, Atmospheric Chemistry
743 and Physics, 16, 1365-1375, https://doi.org/10.5194/acp-16-1365-2016, 2016b.
744 Zhai, S., An, X., Liu, Z., Sun, Z., and Hou, Q.: Model assessment of atmospheric pollution control
745 schemes for critical emission regions, Atmospheric Environment, 124, 367-377,
746 https://doi.org/10.1016/j.atmosenv.2015.08.093, 2016.
747 Zhang, F., Wang, Z. W., Cheng, H. R., Lv, X. P., Gong, W., Wang, X. M., and Zhang, G.: Seasonal
748 variations and chemical characteristics of $PM_{2.5}$ in Wuhan, central China, Science of the Total
749 Environment, 518-519, 97-105, https://doi.org/10.1016/j.scitotenv.2015.02.054, 2015.
750 Zhang, R., Li, Q., and Zhang, R.: Meteorological conditions for the persistent severe fog and haze
751 event over eastern China in January 2013, Science China Earth Sciences, 57, 26-35,
752 https://doi.org/10.1007/s11430-013-4774-3, 2013.
753 Zhang, X. Y., Wang, Y. Q., Niu, T., Zhang, X. C., Gong, S. L., Zhang, Y. M., and Sun, J. Y.:
754 Atmospheric aerosol compositions in China: spatial/temporal variability, chemical signature,
755 regional haze distribution and comparisons with global aerosols, Atmospheric Chemistry and
756 Physics, 12, 779-799, https://doi.org/10.5194/acp-12-779-2012, 2012.

757 Zhao, T., Gong, S., Huang, P., and Lavoué, D.: Hemispheric transport and influence of
758 meteorology on global aerosol climatology, Atmospheric Chemistry & Physics Discussions, 12,
759 https://doi.org/10.5194/acp-12-7609-2012, 2012.
760 Zhao, X. J., Zhao, P. S., Xu, J., Meng, W., Pu, W. W., Dong, F., He, D., and Shi, Q. F.: Analysis of
761 a winter regional haze event and its formation mechanism in the North China Plain, Atmospheric
762 Chemistry and Physics, 13, 5685-5696, https://doi.org/10.5194/acp-13-5685-2013, 2013.
763 Zheng, H., Kong, S., Wu, F., Cheng, Y., Niu, Z., Zheng, S., Yang, G., Yao, L., Yan, Q., Wu, J.,
764 Zheng, M., Chen, N., Xu, K., Yan, Y., Liu, D., Zhao, D., Zhao, T., Bai, Y., Li, S., and Qi, S.:
765 Intra-regional transport of black carbon between the south edge of the North China Plain and
766 central China during winter haze episodes, Atmospheric Chemistry and Physics, 19, 4499-4516,
767 https://doi.org/10.5194/acp-19-4499-2019, 2019.
768 Zhong, J., Zhang, X., Wang, Y., Wang, J., Shen, X., Zhang, H., Wang, T., Xie, Z., Liu, C., Zhang, H.,
769 Zhao, T., Sun, J., Fan, S., Gao, Z., Li, Y., and Wang, L.: The two-way feedback mechanism between
770 unfavorable meteorological conditions and cumulative aerosol pollution in various haze regions of
771 China, Atmos. Chem. Phys., 19, 3287–3306, https://doi.org/10.5194/acp-19-3287-2019, 2019.
772

773

774

775

776 **Table 1.** Correlation coefficients between hourly $PM_{2.5}$ concentrations and near-surface
777 meteorological elements WS (wind speed), T (air temperature), P (air pressure), and RH (relative
778 humidity) in Wuhan in January 2016.

Correlation coefficients	WS	T	P	RH
$PM_{2.5}$	0.10	0.31	-0.47	0.20

779

780

781 **Table 2.** Correlation coefficients of $PM_{2.5}$ concentrations with wind speed (WS) and air
782 temperature (T) in different air quality levels during the study period.

Air quality	$PM_{2.5}$ levels	Number of samples	WS	T
Clean	$PM_{2.5}$ <75 μg m^{-3}	73	-0.20	0.56
Light pollution	75 μg m^{-3}≤ $PM_{2.5}$ <150 μg m^{-3}	135	-0.19	0.15
Heavy pollution	$PM_{2.5}$ ≥150 μg m^{-3}	37	0.41	-0.08

783

784

785

786 **Table 3.** Atmospheric static stability below heights of 200 m in the boundary layer during heavy
787 pollution and clean air periods with anomalies relative to the average over January 2016 in
788 Wuhan.

Period	heavy pollution period	clean air period	monthly average
	($K\ km^{-1}$)	($K\ km^{-1}$)	($K\ km^{-1}$)
Static stability	4.4	13.2	8.6
Anomalies of stability	-4.2	4.6	-

789

790

791 **Table 4.** The relative contributions of regional transport over CEC to three $PM_{2.5}$ heavy pollution
792 periods, P1, P2, and P3, in the YRMB with local contributions.

Contribution rates	P1	P2	P3	Averages
Regional transport	68.1%	60.9%	65.3%	65.1%
Local contribution	31.9%	39.1%	34.7%	34.9%

793

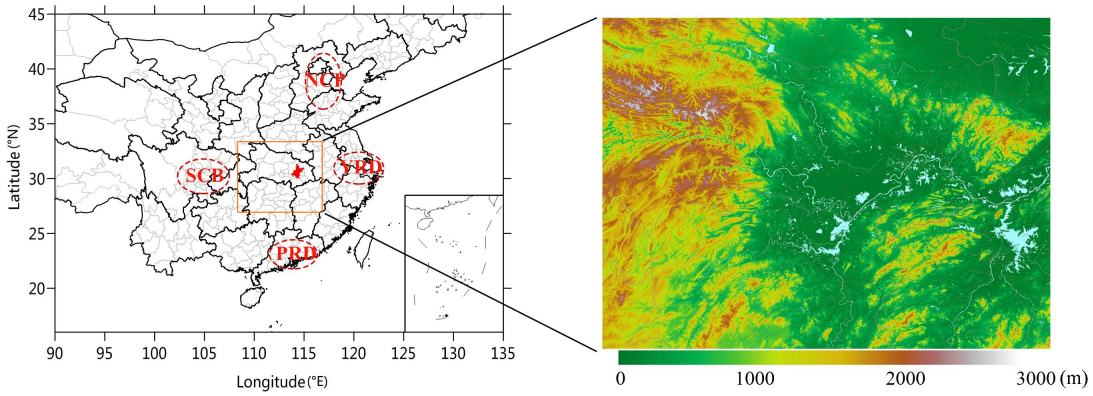

794

795 **Fig. 1.** (a) Distribution of the YRMB (orange rectangle) with the location of Wuhan (red area) and

796 the major haze pollution regions of NCP, YRD, PRD, and SCB in CEC as well as (b) the YRMB

797 region with terrain height (color contours, m in a.s.l.). The river and lake network (blue areas) are

798 downloaded from https://worldview.earthdata.nasa.gov.

799

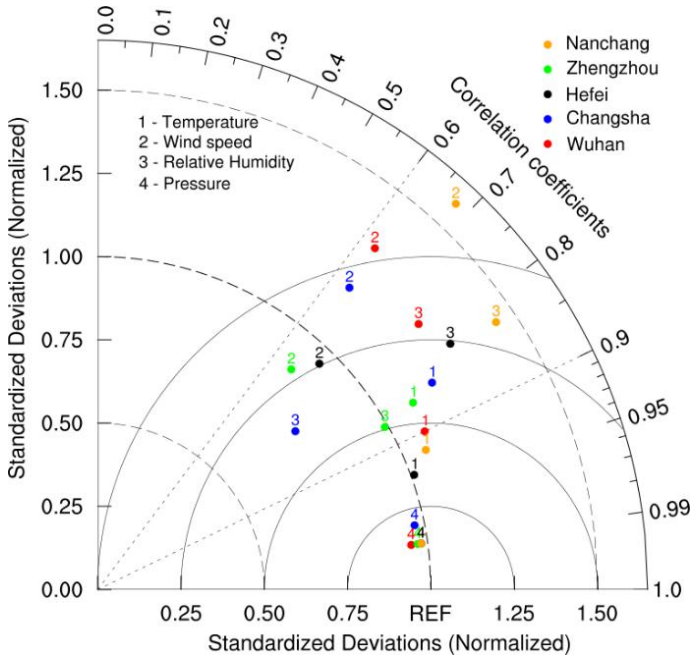

800

801 **Fig. 2.** A Taylor plot with the normalized standard deviations and correlation coefficients between

802 WRF-simulated and observed meteorological fields. The radian of the sector represents the

803 correlation coefficient. The solid line indicates the ratio of standard deviation between simulations

and observations. The distance from the marker to "REF" reflect the normalized root-mean-square error (NRMSE).

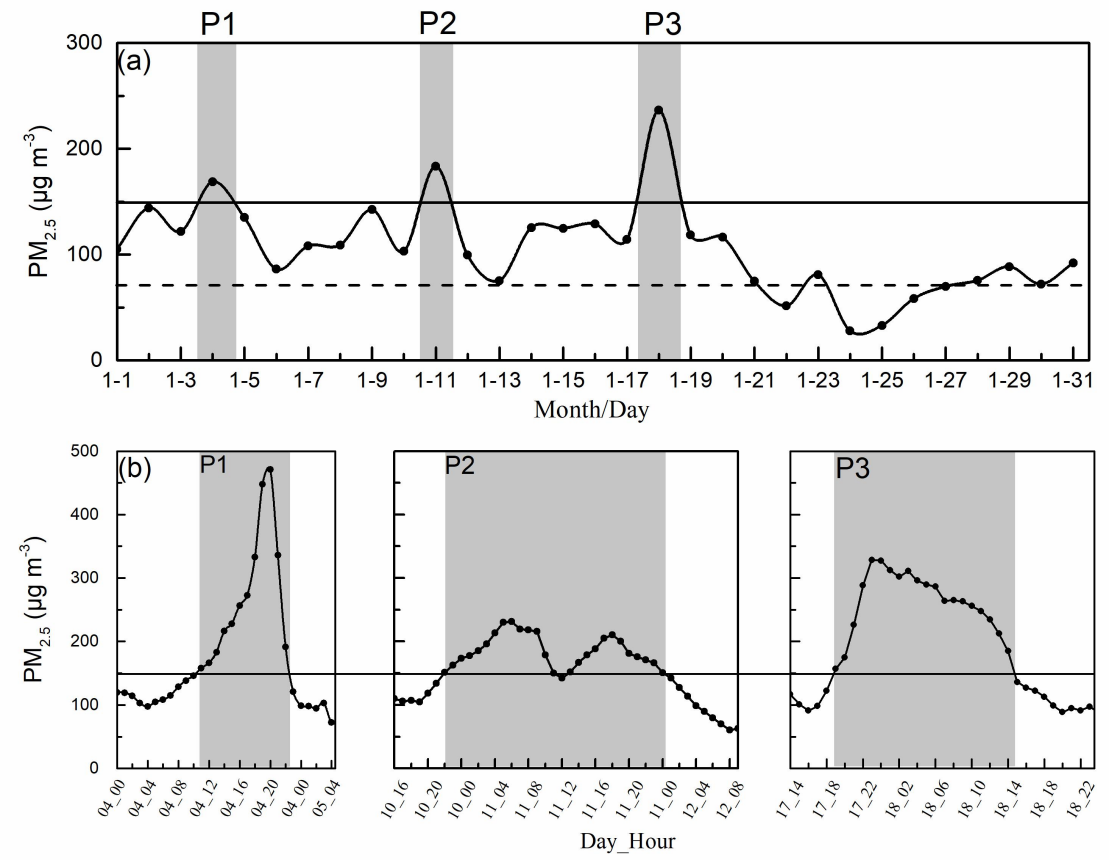

Fig. 3. (a) Daily changes of surface $PM_{2.5}$ concentrations in Wuhan in January 2016 with $PM_{2.5}$ concentrations exceeding 75 μg m^{-3} (dash line) and 150 μg m^{-3} (solid lines) for light and heavy haze pollution, respectively. (b) The hourly variations of surface $PM_{2.5}$ concentrations in three heavy air pollution events, P1, P2, and P3, with excessive $PM_{2.5}$ levels (> 150 μg m^{-3}) marked by the shaded areas.

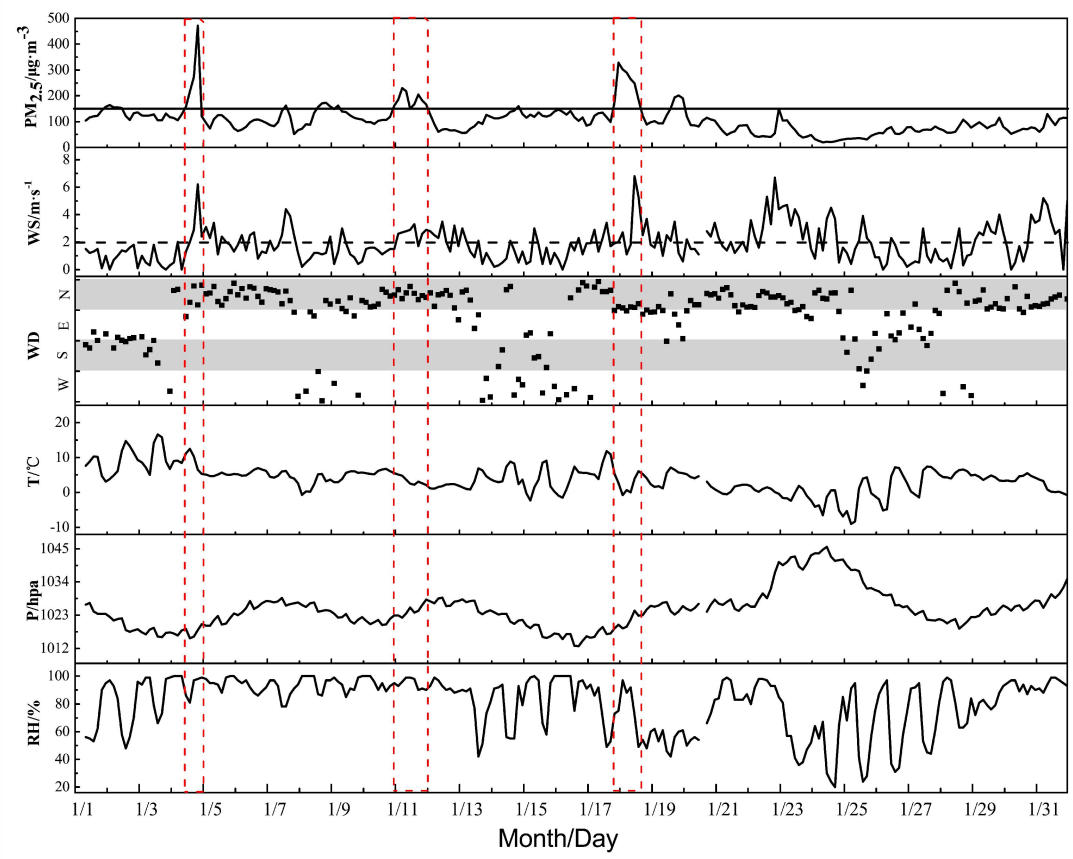

814

815 **Fig. 4.** Hourly variations of meteorological elements and $PM_{2.5}$ concentrations in Wuhan in

816 January 2016. Heavy air pollution periods are marked with columns in red dash lines and $PM_{2.5}$

817 concentrations exceeding 150 μg m^{-3} (solid line in the upper panel).

818

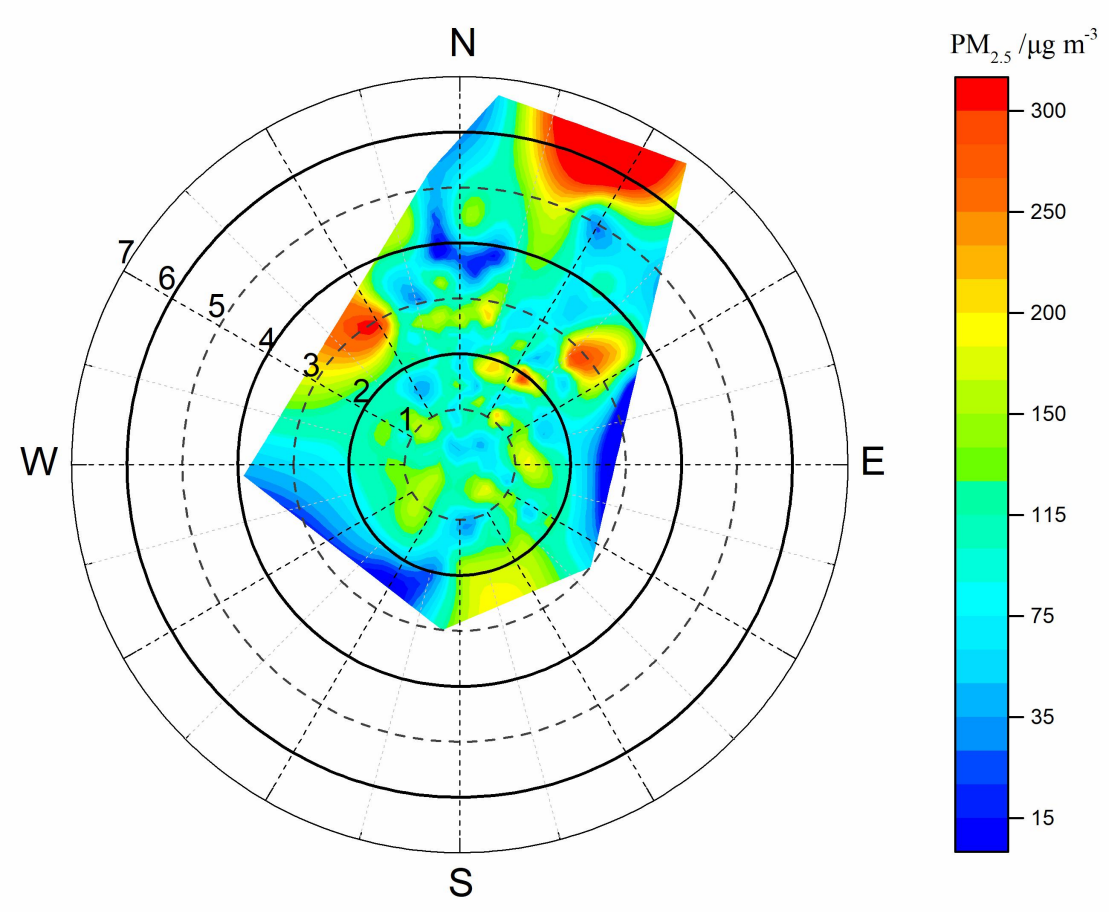

819

820 **Fig. 5.** A polar plot of the hourly variations in wind speed (round radius, in units of m s^{-1}) and

821 direction (angles) to surface $PM_{2.5}$ concentrations (color contours, in units of μg m^{-3}) in Wuhan in

822 January 2016.

823

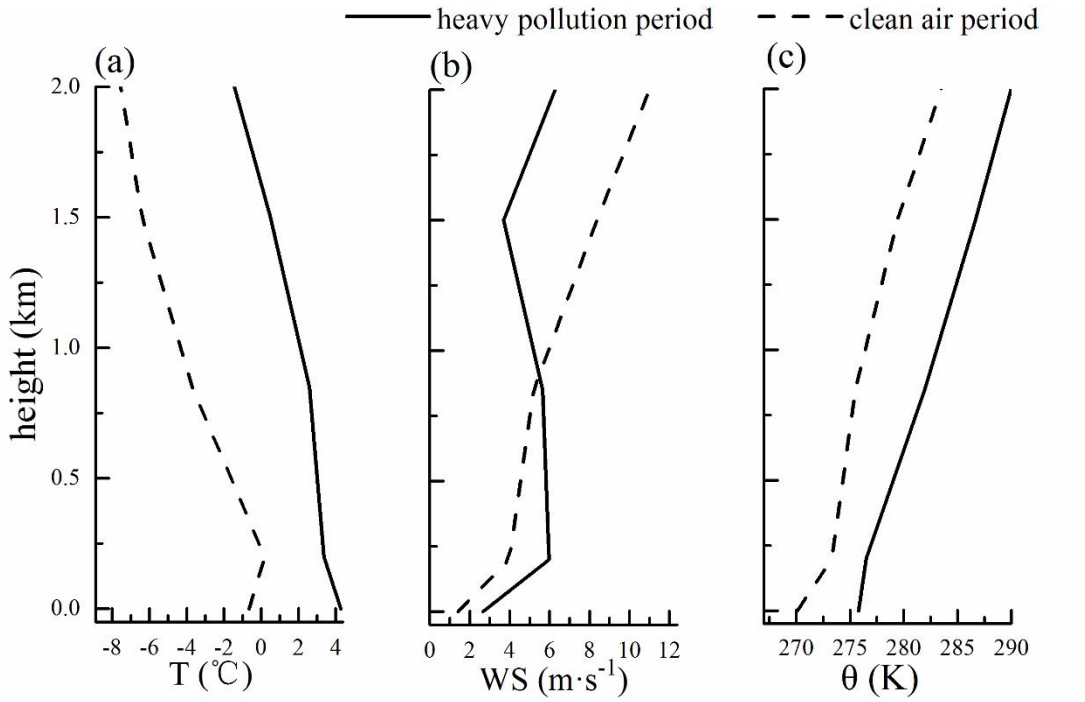

824

825 **Fig. 6.** Vertical profiles of (a) air temperature, (b) wind velocity and (c) potential temperature

826 averaged in the heavy pollution periods P1, P2 and P3 and in the clean air period over Wuhan

827 during January 2016.

828

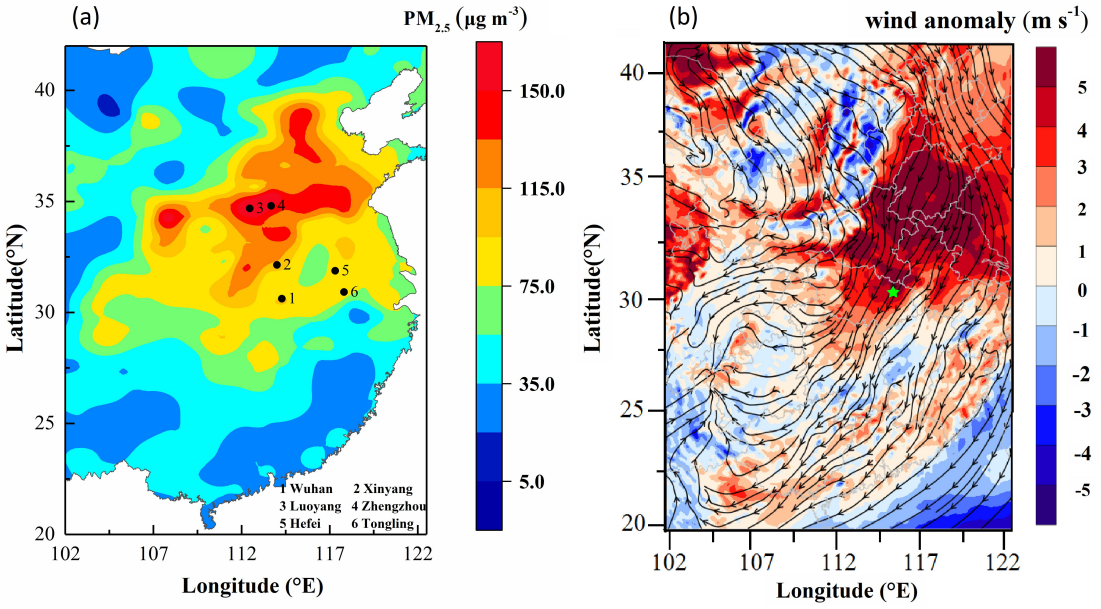

829

830 **Fig. 7** (a) Distribution of the monthly averages of surface $PM_{2.5}$ concentrations observed in

January 2016 over CEC with the locations of six sites (black dots): 1. Wuhan, 2. Xinyang, 3. Luoyang, 4. Zhengzhou, 5. Hefei, and 6. Tongling. (b) Distribution of anomalies (color contours) of 200 m wind speeds averaged during the three heavy air pollution periods relative to the monthly wind averages (streamlines) in January 2016 over CEC with the location of Wuhan (a light blue star).

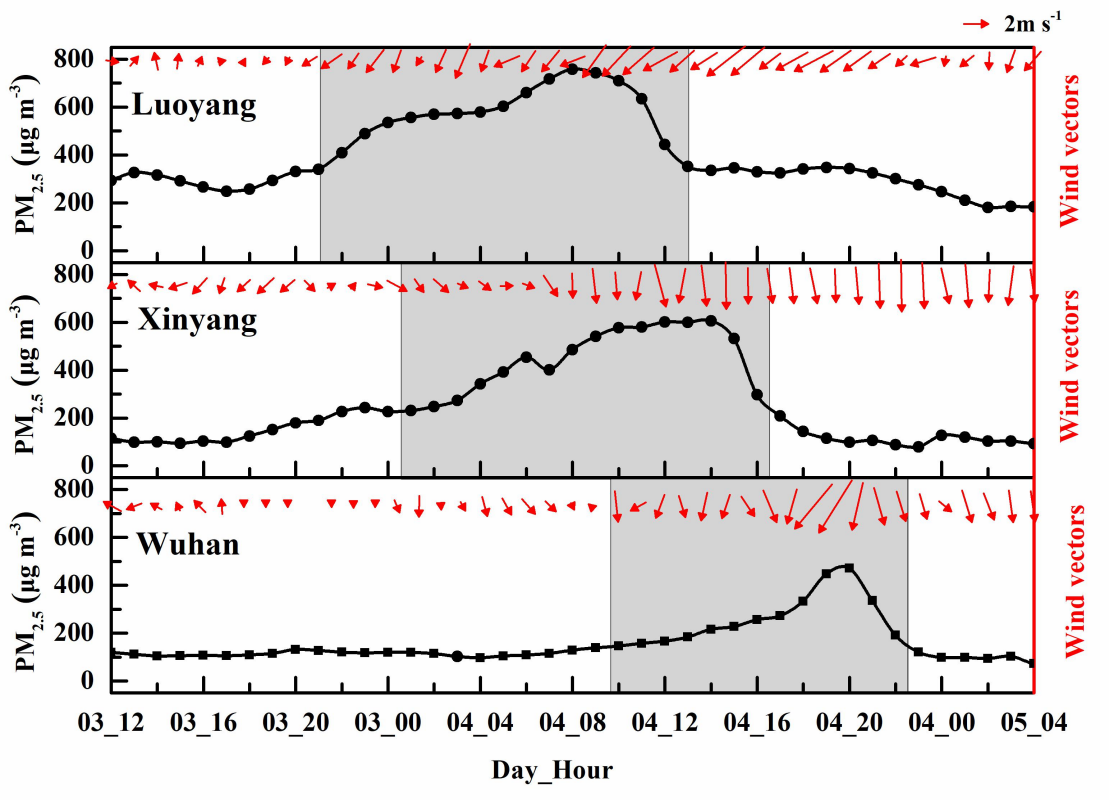

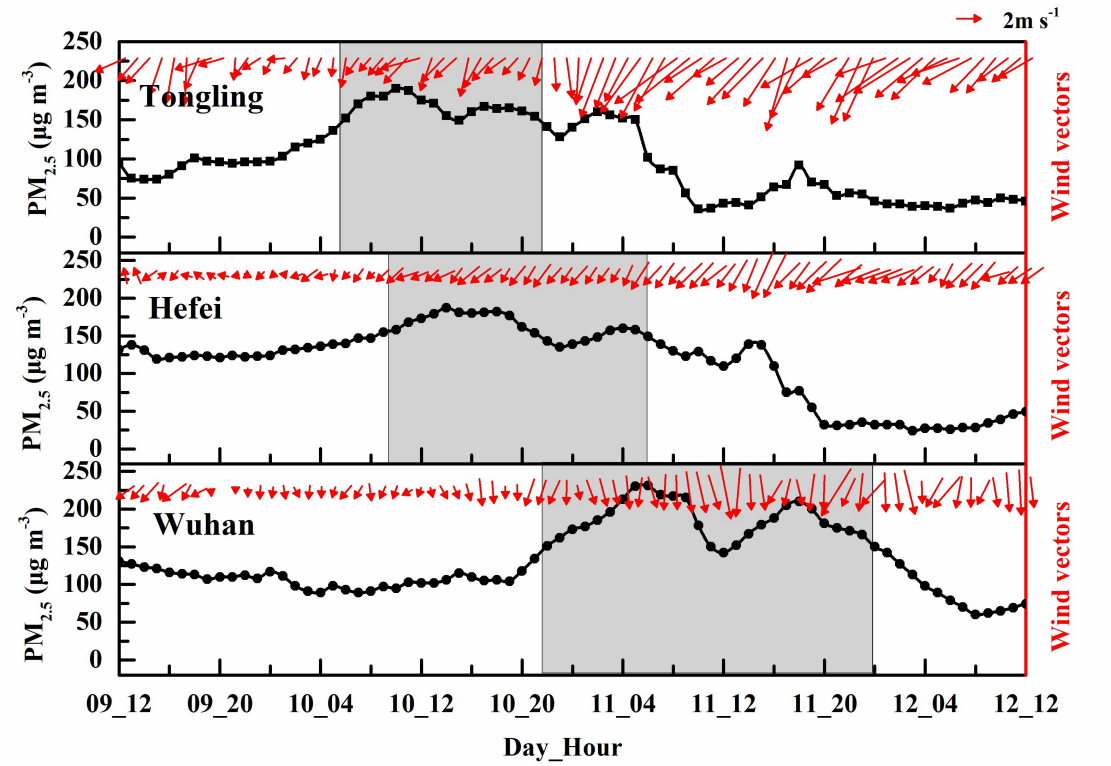

838

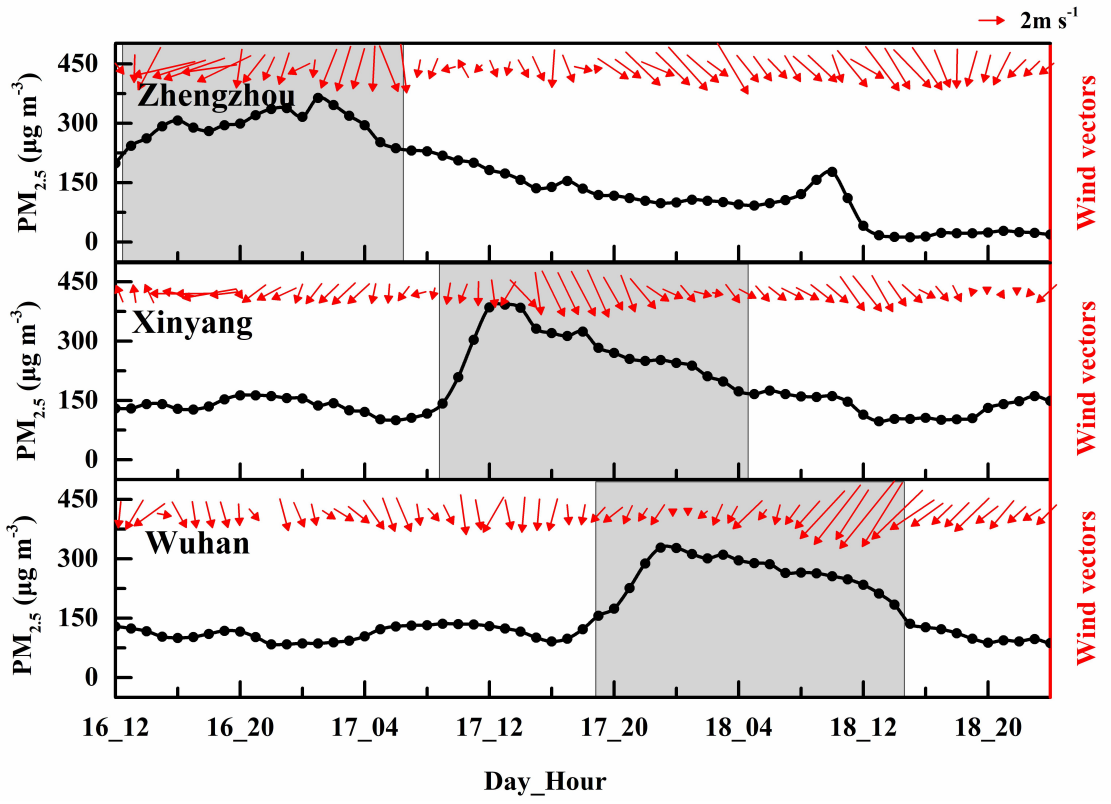

839

840 **Fig. 8.** Temporal changes of $PM_{2.5}$ concentrations (dotted lines) and near-surface winds (vectors)

841 observed at five upstream sites (Fig. 6) and Wuhan with shifts of $PM_{2.5}$ peaks (marked with shaded

842 areas) to the YRMB's heavy $PM_{2.5}$ pollution periods P1 (upper panel), P2 (middle panel) and P3

843 (lower panel), in January 2016.

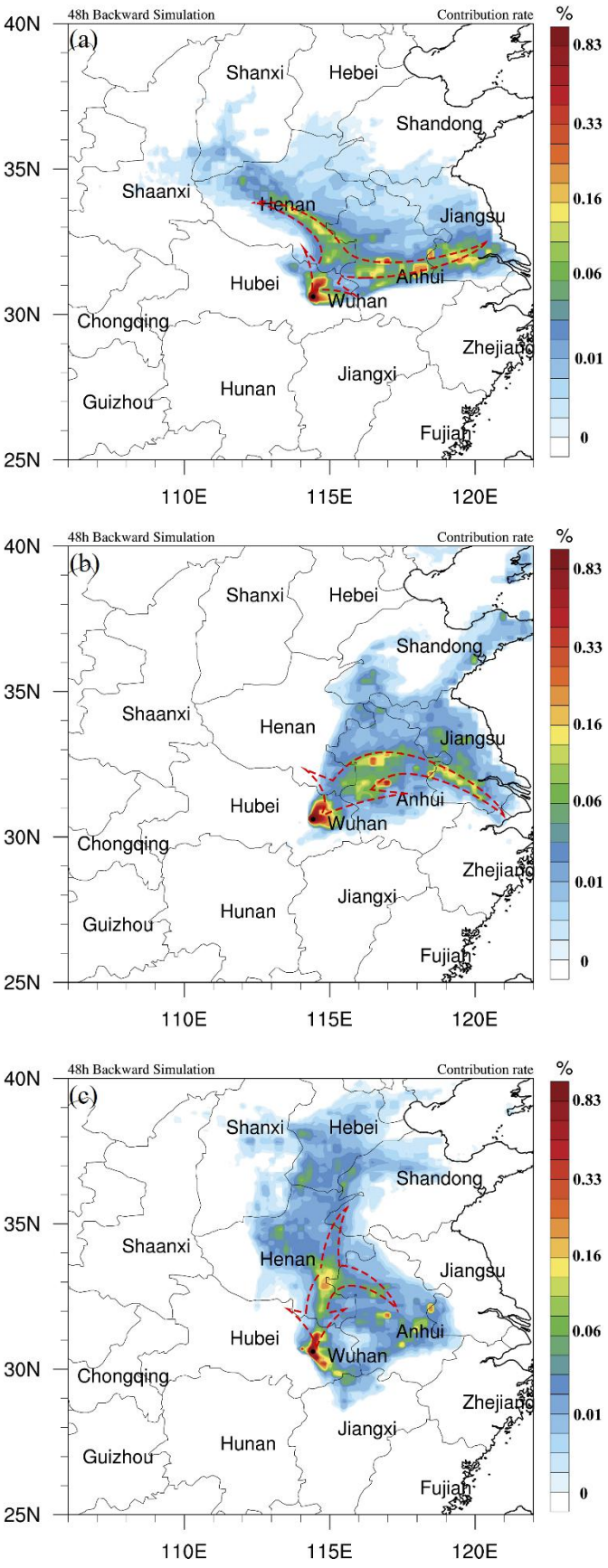

844

845 **Fig. 9.** Spatial distribution of contribution rates (color contours) to $PM_{2.5}$ concentrations in Wuhan

with the major pathways of regional transport over CEC (dash arrows) for three heavy pollution periods (a) P1, (b) P2, and (c) P3 in January 2016 simulated by the FLEXPART-WRF model.